Available online at www.sciencedirect.com

jmr&t Journal of Materials Research and Technology

journal homepage: www.elsevier.com/locate/jmrt

Original Article

Micro-mechanical response of ultrafine grain and nanocrystalline tantalum

Wen Yang [a], Carlos J. Ruestes [b], Zezhou Li [a], Oscar Torrents Abad [c], Terence G. Langdon [d], Birgit Heiland [c], Marcus Koch [c], Eduard Arzt [c,e], Marc A. Meyers [a,*]

[a] University of California, San Diego, USA
[b] CONICET - Universidad Nacional de Cuyo, Mendoza, Argentina
[c] INM – Leibniz Institute for New Materials, Saarbrücken, Germany
[d] University of Southern California, USA
[e] Saarland University, Saarbrücken, Germany

ARTICLE INFO

Article history:
Received 19 August 2020
Accepted 19 March 2021
Available online 25 March 2021

Keywords:
Micropillar
Nanocrystalline
Tantalum

ABSTRACT

In order to investigate the effect of grain boundaries on the mechanical response in the micrometer and submicrometer levels, complementary experiments and molecular dynamics simulations were conducted on a model bcc metal, tantalum. Microscale pillar experiments (diameters of 1 and 2 μm) with a grain size of ~100–200 nm revealed a mechanical response characterized by a yield stress of ~1500 MPa. The hardening of the structure is reflected in the increase in the flow stress to 1700 MPa at a strain of ~0.35. Molecular dynamics simulations were conducted for nanocrystalline tantalum with grain sizes in the range of 20–50 nm and pillar diameters in the same range. The yield stress was approximately 6000 MPa for all specimens and the maximum of the stress–strain curves occurred at a strain of 0.07. Beyond that strain, the material softened because of its inability to store dislocations. The experimental results did not show a significant size dependence of yield stress on pillar diameter (equal to 1 and 2 um), which is attributed to the high ratio between pillar diameter and grain size (~10–20). This behavior is quite different from that in monocrystalline specimens where dislocation 'starvation' leads to a significant size dependence of strength. The ultrafine grains exhibit clear 'pancaking' upon being plastically deformed, with an increase in dislocation density. The plastic deformation is much more localized for the single crystals than for the nanocrystalline specimens, an observation made in both modeling and experiments. In the molecular dynamics simulations, the ratio of pillar diameter (20–50 nm) to grain size was in the range 0.2–2, and a much greater dependence of yield stress to pillar diameter was observed. A critical result from this work is the demonstration that the important parameter in establishing the overall deformation is the ratio between the grain size and pillar diameter; it governs the deformation mode, as well as surface sources and sinks, which are only important when the grain size is of the same order as the pillar diameter.

* Corresponding author.
E-mail address: mameyers@eng.ucsd.edu (M.A. Meyers).

https://doi.org/10.1016/j.jmrt.2021.03.080

1. Introduction

Micrometer and sub-micrometer compression experiments have played, since their introduction by Uchic et al. [1] and Greer et al. [2], a significant role to probe the response of metals at that scale. Gradient theory, first proposed by Ashby [3] and analytically developed by Aifantis [4] and Nix and Gao [5], predicts a strain gradient-dependent strength and helps explain experimental results in torsional specimens where the strain is zero at the neutral axis (coincident with the symmetry axis in cylindrical specimens) and maximum at the surface [6]. This behavior is contrary to classical plasticity where strength is independent of scale. The geometry of loading is quite different in micropillar experiments, where there is no imposed strain gradient.

Micromechanical compression tests were enabled by focused ion beam technology (for specimen preparation) followed by compression in a nanoindenter (or similar instrument) with a flat punch. Provided that the friction between the sample and the punch is negligible, there is no geometrically-imposed strain gradient and the state of stress is uniaxial compression. The surprising result obtained by Greer et al. [2], a strong scale dependence for monocrystalline gold, was attributed to dislocation 'starvation'. As the diameter decreases, dislocations, driven by the image forces, are closer and attracted to the free boundary, which acts as a sink. Thus, existing dislocations vanish, inhibiting conventional multiplication processes. This seminal work on gold was followed by an avalanche of papers, which confirmed the effect for a number of metals. In subsequent work, Kim et al. [7] investigated <001> monocrystalline tantalum in both tension and compression. The strength/specimen size effect, obtained as the slope of the logarithm of a normalized strength vs. normalized diameter, was found to be −0.44.

In order to determine whether possibly strain gradients exist within the material, Budiman et al. [8] used submicrometer size Laue X-Ray diffraction. They found no evidence of strain gradients in Au, even at a strain of 0.35. Thus, the increase in strength with decreasing dimensions has to be ascribed to the absence of dislocations, after the ones existing are expelled to the surface by the applied stress and image forces. Indeed, this increase in strength for reduced dimensions has been known for a long time and is a characteristic of whiskers. An iron whisker with a diameter of 3 μm has a strength of G/17, close to the theoretical value [9,10]. When this stress is exceeded, there is a sudden drop in load as dislocations are nucleated inside the crystal.

In the present paper, compression experiments were conducted on micropillars, with diameters 1 and 2 μm, of tantalum with grain size of 100–200 nm. These experiments were complemented by molecular dynamics simulations. The aim of the present work was to establish whether the pillar diameter or the grain size determines the strength of a micropillar made of a bcc metal with an ultrafine grain structure, where there is a profuse availability of internal dislocation sources and sinks in contrast with monocrystals. The reason for using monocrystalline Ta as the starting material was to ensure that the composition was identical to that of the previously studied monocrystalline Ta, thus enabling a direct comparison [11,12].

2. Experimental methods

2.1. Achieving nanocrystalline grain size

Nanocrystalline Ta was prepared by high-pressure torsion (HPT) processing from [100] monocrystalline Ta. Pure monocrystalline Ta was obtained from MarkeTech Intl, Inc. The interstitial content (ppm in weight) for the monocrystalline Ta was analyzed as O: <10, N: <10, H: 7.6 and C: <10 by standard SIMS at the Evans Analytical Group.

High Pressure Torsion was conducted at room temperature using a quasi-constrained torsional machine with upper and lower anvils having a cylindrical depression at the center of adjacent surfaces with a depth of 0.25 mm and a diameter of 10 mm [13], onto which the sample was placed. All samples were processed at a pressure of 6 GPa for a total of 6 turns at a rotational speed of 1 rpm. As a result of the torsion, the disk dimensions changed from 10 to ~10.5 mm diameter and 1 to 0.75 mm thickness due to outflow around the periphery. The micro-hardness increases from the center of the disc to its perimeter and becomes uniform after a radius of about 5 mm. The compression specimens were prepared from the region with uniform hardness.

2.2. Micropillar preparation

To identify the size effect as well as the strain-rate-sensitivity of the nanocrystalline Ta samples, small compression pillars were machined via focused ion beam (FIB) milling into the surface of the bulk nanocrystalline sample. The advantage of this technique is that both of the location and the size of the samples can be well controlled.

An FEI Versa 3D Dual Beam (Hillsboro, OR) microscope combining an SEM and FIB was used. The pillar samples were fabricated using this FIB system under a coarse milling condition of 30 kV and 15 nA and a final polishing condition of 30 KV and 0.3 nA or 0.1 nA. Samples with diameters of 1 and 2 μm and aspect ratio (height: diameter ratio) of 3:1 were prepared in two steps. First, coarse pillars were milled by using the circular milling patterns with an outer diameter of 30 μm to ensure a large surrounding area where the edges would not be touched by the indenter during the compression tests. Afterwards, a fine milling procedure was carried out at low currents in order to reduce the gallium ion damage of the pillars and to adjust the final size of the pillars to the nominal aspect ratio. Some of the pillars were refined by lower current to ensure a small difference between the diameters from the top surface to the bottom of the pillars.

2.3. Micro-compression testing

The FIB-milled pillars were compressed uniaxially using a custom-modified in situ Hysitron stage built with a Vickers shape indenter (diagonal size of ~10 micron) with a 30 mN load cell in the same FIB-SEM system in vacuum, at pressures

between 10^{-6} and 10^{-5} mbar. Compression tests were carried out at strain rates of 10^{-4}/s and 10^{-3}/s until reaching a relative compression of 30% of the sample height.

2.4. Molecular dynamics methods

Molecular dynamics (MD) simulations of polycrystalline nanopillars were performed as a computational microscopy technique [14] to provide further insights into the plasticity mechanisms taking place. 3D nanoscale pillars were cut out, in the computer, from bulk Ta polycrystals generated using Atomsk [15], with random crystallographic orientations. Four polycrystals were built, with average grain sizes of 20, 30, 40 and 50 nm, in a simulation domain of $80 \times 80 \times 150$ nm^3. Four nanopillars were cut out from each polycrystal, with dimensions of 20, 30, 40 and 50 nm diameter at medium height and an aspect ratio of 3 and a taper angle of 2.5°. The 20 nm diameter pillar contained 1 million atoms, while the 50 nm diameter pillar contained approximately 16 million atoms. Each pillar was energetically minimized and then relaxed for 40 ps at zero pressure and 300 K. The lateral surfaces of the MD specimens do not have any imperfections.

The compression was performed by means of an indenter with a planar face [16]. Two atom layers at the bottom of the pillar were fixed in order to prevent any rigid-body movement of the sample. The simulations were performed in an NPT ensemble at a temperature of 300 K. The atomic interactions were modeled using the extended Finnis-Sinclair potential by Dai et al. [17], extensively used for Ta MD simulations [18–20]. The indenter plane was initially placed at a distance $z > R_{cut}$ above the pillar uppermost surface such that the indenter had no interaction with it, R_{cut} being the potential cut-off radius. Then the indenter was pushed in the direction perpendicular to the top of the pillar, at a speed of 20 m/s, which is approximately 0.006 C_0, where C_0 is the directionally-averaged sound velocity in Ta. The simulation was performed in the displacement-controlled mode: at every MD time step Δt, the indenter proceeded rigidly by a path length $v \cdot \Delta t$. The indenter compressed the pillar until a maximum deformation of 15% was achieved. This maximum deformation was limited by the available computational resources.

Simulations were performed using the Large Scale Atomic/Molecular Massively Parallel Simulator (LAMMPS) [21] with a time step of 0.002 ps. In addition, OVITO [22] was used for visualization and post processing.

3. Results and discussion

3.1. Microstructure of nanocrystalline tantalum prior to and after deformation

The structure generated by high pressure torsion had a grain size of approximately 100 nm. The grains were virtually free of dislocations but not entirely equiaxed, having an aspect ratio of ~2. The characterization by TEM is shown in Fig. 1. The formation of nanocrystalline grain structures by severe plastic deformation has been well described in the literature and is an accepted experimental method. This structure lends itself well to the proposed experiments because the grain size is lower, by approximately one order of magnitude, than the pillar diameter [23].

3.2. Mechanical response

Fig. 2 shows the compressive stress–strain curves resulting from two tests each on the two pillar diameters (1 and 2 μm) and at two strain rates (10^{-3} and 10^{-4} s^{-1}). The effect of strain rate cannot be clearly distinguished because it is masked by the variability of the individual tests. The curves show work hardening that gradually decreases to zero at a strain of 0.25. Inserts show two of the pillars after compression with some indication of buckling. The yield stresses lie in the range 1500 to 1800 MPa, with no clear effect of the diameter. The nanocrystalline micro-pillars hence exhibit strength values that are significantly higher than the values reported for conventional polycrystalline Ta (>1300 MPa) when processed by HPT for 5 turns under the same applied pressure of 6 GPa [24].

The stress–strain curves can be compared with the result of the work from the Wei group [25,26] on Ta subjected to a similar high-pressure torsion process (number of turns of 5 in comparison with 6 turns in the current work). The flow stresses of the nanocrystalline pillars are fairly similar, as shown in Fig. 3a. In contrast, monocrystalline Ta [27] behaves in a radically different manner: Some curves show serrations typical of single-crystalline micropillars and the flow stress decreases with increasing pillar diameter. The dependence of yield stress on pillar diameter was interpreted by Abad et al. [27] in terms of dislocation starvation. As the diameter is decreased, dislocations escape more easily and have less of an opportunity to interact and to multiply by conventional mechanisms. Thus, the monocrystals become devoid of dislocations and the strength increases. As the diameter is increased, dislocations travel farther before reaching the surface and have a greater opportunity to interact and

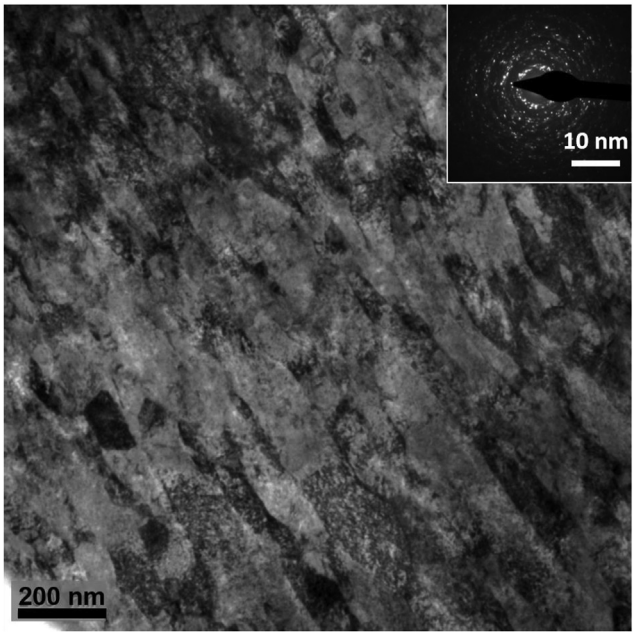

Fig. 1 – Nanocrystalline structure of tantalum produced by high pressure torsion. The grain size is about 100 nm. Note the slight elongation of the grains from upper left to lower right.

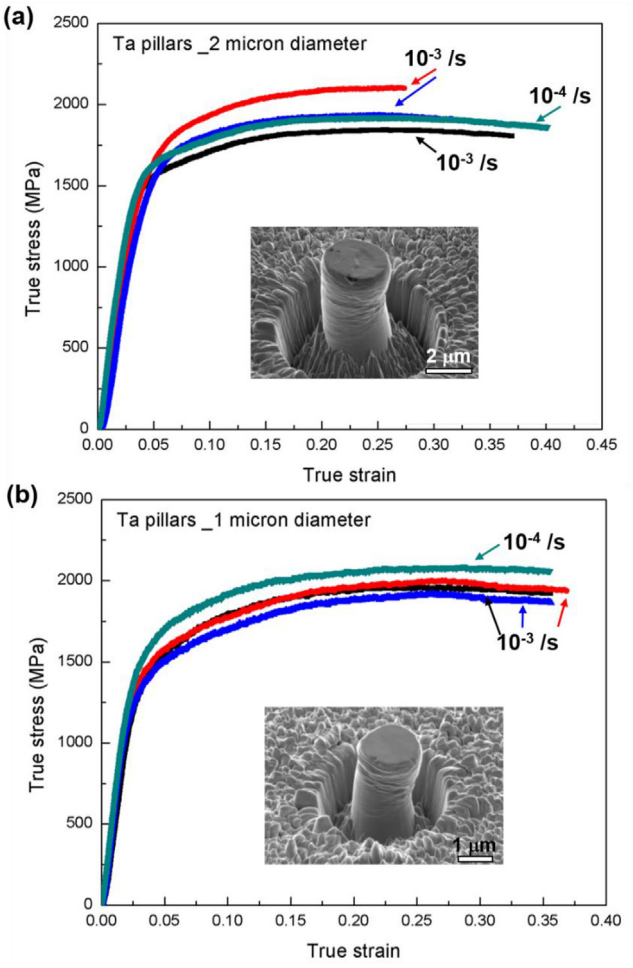

Fig. 2 – Stress strain curves for two different pillar diameters (1 and 2 μm) and two strain rates (10^{-3} and 10^{-4} s^{-1}). The results of two tests under each condition are shown. The effects of pillar diameter and of strain rate are small.

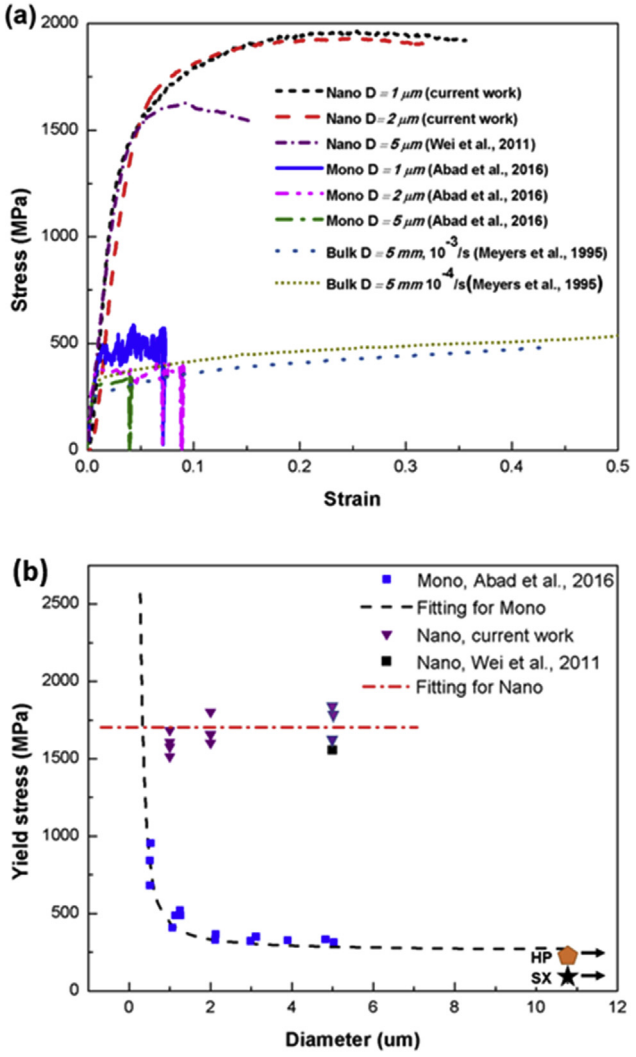

Fig. 3 – Effect of pillar diameter on yield stress of monocrystalline (from Abad et al. [27]) and nanocrystalline (current results and Wei et al. [25]); (a) stress–strain curves; (b) yield stress vs. pillar diameter; note the strong size dependence in monocrystalline and weak dependence in nanocrystalline tantalum. Specimen with 3 mm diameter indicated by arrow (SX: single crystal [28]; HP: σ_0 extracted from $\sigma = \sigma_0 + kd^{-1/2}$ [20–31]).

multiply. The mechanical response of the Ta monocrystal in the D = 5 μm pillar is fairly similar to that of bulk specimens having dimensions three orders of magnitude higher: the two extended curves, up to compressive strains of 0.4, are shown in the bottom of Fig. 3a; these specimens have a diameter of 3 mm and a grain size of 31 μm, larger than the micropillars. Fig. 3b shows the yield stresses of the specimens as a function of pillar diameter. The response of the nanocrystalline material is again drastically different from the monocrystal. Most importantly, the yield stress of the nanocrystalline specimens is constant at about 1600 MPa. For comparison purposes, we include yield stress values for 1.9 mm single crystals under compression [28], together with an estimated value of σ_0 for a typical Hall Petch behavior ($\sigma = \sigma_0 + kd^{-1/2}$) (after data of Zerilli and Armstrong [29,30]).

The stress–strain response of a polycrystal is reproduced in Fig. 3a for comparison with the ultrafine grained material. It can be seen that the work hardening rate is sustained to high strains. The saturation of hardening of the ultrafine grain material is due to its inability to accumulate higher dislocation densities because of the ready availability of sinks (the grain boundaries). In polycrystals the dislocations interact inside of the grains and their density increases. This leads to work hardening, described by Taylor's equation: $\sigma = k\rho^{0.5}$, where ρ is the dislocation density. The monotonic work hardening up to a strain of 0.4 is shown in Fig. 3a.

The significant difference in the results is due to the fact that in fine-grained structures only a small fraction of dislocations can escape to the surface. Similar results were obtained in a dispersion-strengthened superalloy by Girault et al. [32]. In this case deformation was controlled by internal obstacles and not by the surface effects such as dislocation starvation. They obtained a very small dependence of strength on pillar diameter, which was varied from 0.2 to 4 μm.

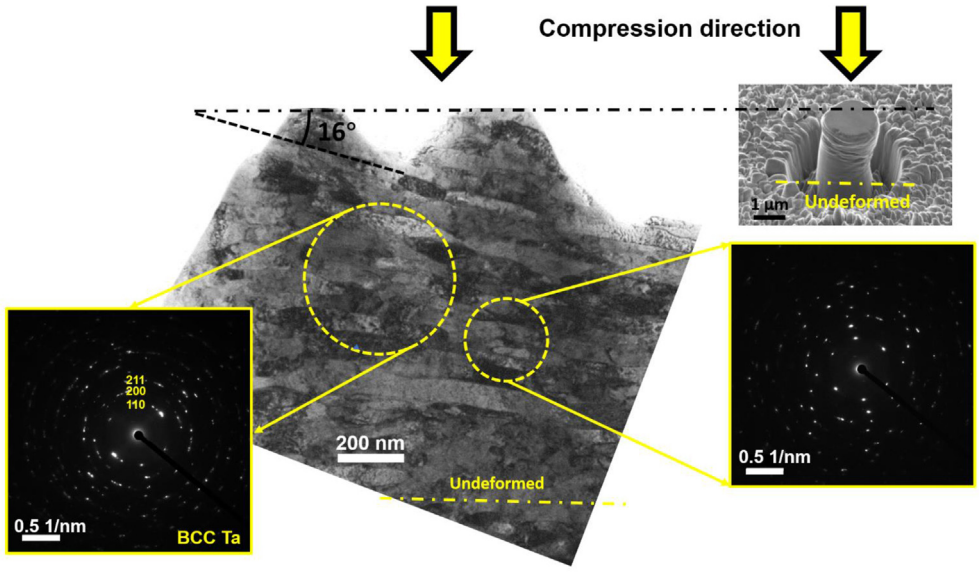

Fig. 4 – Post deformation grain structure of nanocrystalline tantalum; note deformation of grains into 'nano-pancakes' by compressive deformation.

3.3. *Characterization of the deformed samples*

Figs. 4 and 5 show TEM micrographs of specimens after compression testing. The deformed material consists of elongated nanosized grains. In the dark field micrograph (Fig. 5b), one can see a low-angle grain boundary. On the other hand, the bottom of the micrograph in the central picture of Fig. 4 shows grains that are less elongated. This can be partially accounted for by plastic deformation of the grains to a strain of ~0.4 and partially by the initial structure that is not quite equiaxed. There was some initial anisotropy in the grain structure created by SPD, evident in Fig. 1. Assuming that the initial aspect ratio is 2:1, approximate constancy in volume (Poisson ratio of Ta is 0.34) would result in a flattening of the grains to an aspect ratio of 4:1 at this strain.

Additional details of the deformed grains are revealed in Fig. 5. They are clearly elongated, as is seen in the dark field micrograph of Fig. 5b and one can see (Fig. 5c) a low-angle grain boundary dividing an elongated grain into two.

3.4. *Molecular dynamics predictions of stress strain response for nanocrystalline tantalum*

Fig. 6a shows the MD prediction for a nanocrystalline specimens of grain size of 20 nm and pillar diameters of 20–50 nm. Fig. 6b shows the same for a constant average grain size of 50 nm. It is seen in Fig. 6a that the maximum stress is insensitive to pillar diameters if they exceed the grain size. One can conclude from this that, if the grain size is significantly smaller than the pillar diameter, deformation is controlled by emission and annihilation of dislocations at grain boundaries, the free surface of the pillar not playing an important role.

By contrast, we can see in Fig. 6b that the maximum stress increases as the pillar diameter rises towards the grain size. This is very likely due to the fact that grain boundaries act as nucleation sites for dislocations; as the grain size approaches the pillar size, there is a lower density of nucleation sites. A noticeable feature is that the 20 nm grain size pillar undergoes much more rapid softening, i.e. a decrease beyond the maximum stress. This behavior is accompanied by a pronounced localization of shear, which will be discussed in Section 3.5.

One has to realize that MD limitations do not enable a direct comparison with experimental results. There is a drastic difference in strain rates: in the MD calculations presented herein it is 10^7 s^{-1}, which is ten orders of magnitude higher than in the experiments. These differences in grain size and strain rate are reflected in the maximum stress of 1.5 GPa for the experiments vs. 6 GPa for the simulations. Despite the limitation of molecular dynamics, fundamental mechanisms can nevertheless be revealed.

The MD yield stresses were extracted from the stress–strain data at a strain offset of 1% due to the slight nonlinear elastic regime (Fig. 7). A [001]-oriented single crystal pillar and a [111]-oriented single crystal pillar with 50 nm diameter and the same taper angle and aspect ratio were loaded in the same way as the nanocrystalline samples. The resulting single-crystal stress strain curves are almost linear in the range of strain in which the nanocrystalline samples were nonlinear elastic (not shown for simplicity). We attribute the nonlinear elasticity in the latter to grain boundary activity; a similar effect was reported by Gu et al. [33] in their study of nanocrystalline Pt pillars. The 1% strain offset yield stresses are compiled and reported in Fig. 7a in terms of pillar diameter (D), in Fig. 7b in terms of grain size (d), and in Fig. 7c in terms of grain size to pillar diameter ratio (d/D).

Three-dimensional variables might play a role in the strength of pillars, albeit in a different proportion. These are the pillar diameter effect, the grain size effect, and the aspect ratio (d/D) effect. Attempts have been made to capture these three influencing terms using a linear superposition of effects, such as was done by Chen and Ngan [34], whose model can be recast as, for samples showing a Hall–Petch effect with respect to grain size:

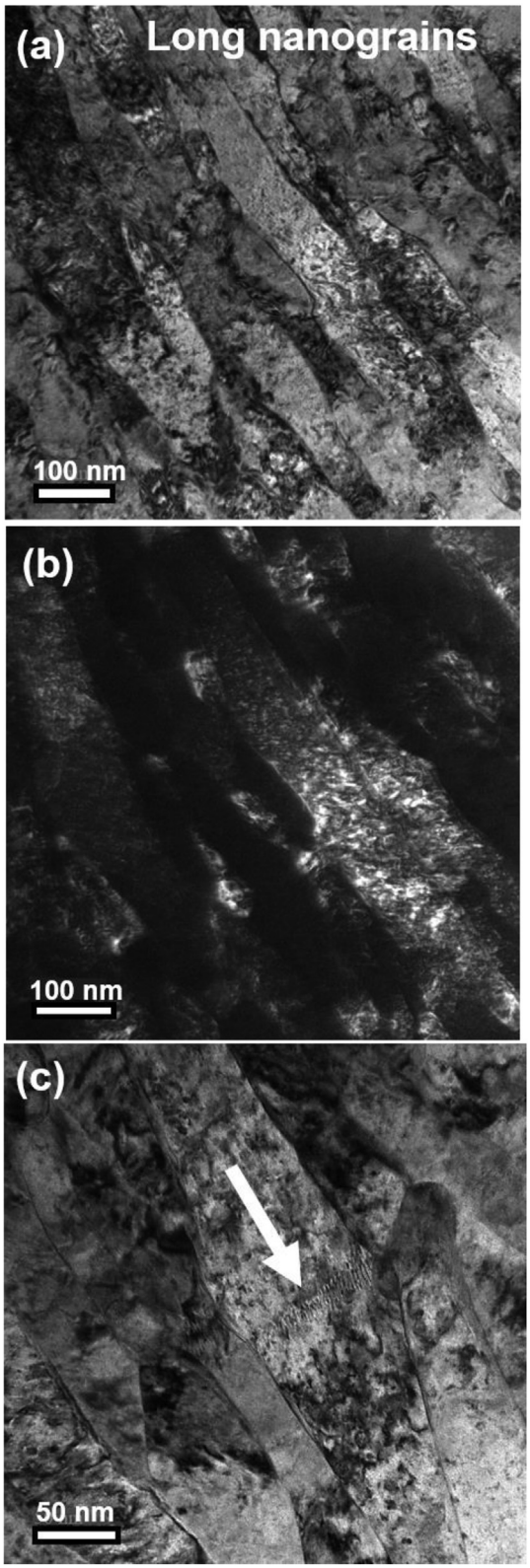

Fig. 5 – Post compression grain structure and dislocation activity in nanocrystalline specimen (2 μm pillar at 10^{-3} s^{-1}). (a) bright field; (b) dark field; (c) arrow pointing at low-angle grain boundary initiating separation.

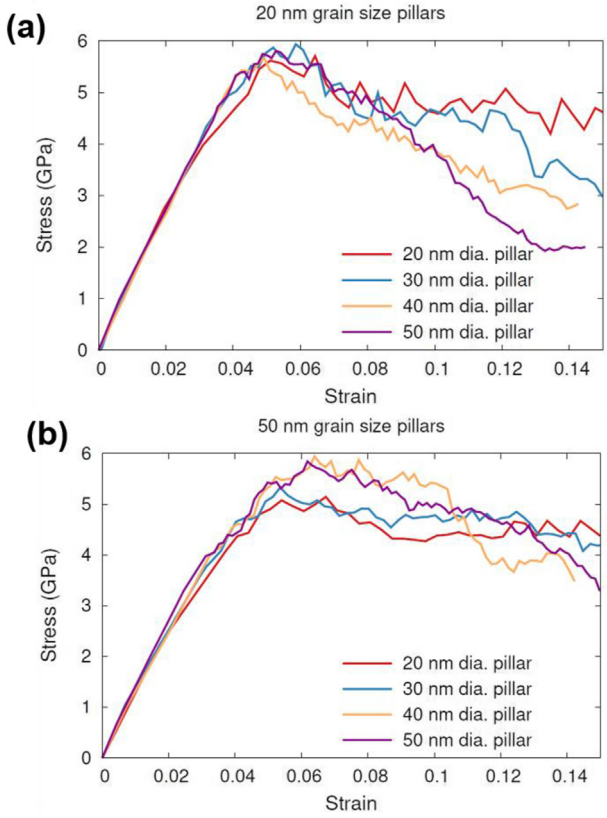

Fig. 6 – Molecular dynamics simulations of nanocrystalline tantalum with (a) 20 nm and (b) 50 nm grain size and different pillar diameters (10–50 nm).

$$\sigma_y = \sigma_1\,(D) + \sigma_2\,(d\,/\,D) + kd^{(-1/2)} \tag{1}$$

A similar approach was taken by Yuan et al. [35] for samples displaying an inverse Hall–Petch effect, but adding a randomness correction term.

$$\sigma_y = \sigma_1\,(D) + \sigma_2\left(\frac{d}{D}\right) + kd + \Delta\sigma \tag{2}$$

Neither of these two expressions are fully applicable to the data set presented here, as our results show a H–P effect for grain size in the range of 40–50 nm and do show a plateau for grain sizes in the 30–20 nm range. In addition, there is no clear dependence on the pillar diameter (D) (Fig. 7a), whereas there is a dependence on the grain size, shown in Fig. 7b. As a consequence, our yield stress computation results depict a rather weak dependence on d/D ratio (Fig. 7c). As will be seen below, the influence of the aspect ratio becomes fundamental on the deformation patterns.

The computational results could also be interpreted in terms of core–shell effects, considering the model by Gu et al. [33]:

$$\sigma_y = \sigma_y^{bulk}\,(1 - d/D)^2 + \sigma_y^{surf}\left[1 - (1 - d/D)^2\right] \tag{3}$$

where σ_y is the yield stress of the pillar, σ_y^{bulk} that of the bulk material and σ_y^{surf} is the flow stress of the material at the surface. It must be noted that considering σ_y^{bulk} and σ_y^{surf} fixed, Eq. (3) implies that for a given d/D, the yield stress should be the same, regardless of the pillar diameter or the grain size. As d/D tends to zero, such as in the case of samples with the smallest grain size, the nanopillar yield stress approaches that of the bulk material Even though the grains adjacent to the surface possess an effective flow stress that is lower than the material in the interior (grain boundary sliding dominates), the total load carried by grains in the surface region is much smaller than that carried by the pillar interior, due to the relatively smaller grain size and the less constrained plastic deformation of the superficial grains. As a consequence, flow properties (dislocation plasticity) of the nanopillar interior control the deformation. On the other hand, when the grain size is commensurate to the nanopillar diameter, the free surfaces are expected to play a major role, and the yield strength approaches that of the grains in the surface; the flow stress for grain boundary sliding is lower than that associated with bulk nanocrystal dislocation plasticity. Our MD simulations reveal a weak dependence on d/D ratio for the yield stress, the 50 nm pillars being a notable exception, as seen on Fig. 7c, where for a d/D = 1, the 50 nm D pillar yields at a lower stress.

Fig. 7a shows an interesting predicted trend: the largest grain size, d = 50 nm, shows a reduction in yield stress with increasing pillar diameter, whereas the smaller grain sizes do not show the same clear effect. A possible interpretation is that the large grain size resembles the single crystal pillar the most, and therefore surface sources can lead to starvation. With decreasing grain size, the grain boundary area per unit volume increases and hence the relative importance of the surface decreases. Fig. 7b reveals that, as the grain size decreases, the yield strength increases, in a Hall–Petch type behavior. Stresses are of the order of the values reported by Hagen et al. [36] for their MD simulations of α-Fe 50 nm diameter pillars. Our yield stresses for the 20 nm grain size pillars are around 15% lower than the ones reported by Tang et al. [20] for their polycrystalline uniaxial compressive high-strain rate simulations using the same interatomic potential. Such deviations are not untypical as previous studies on nanocrystalline fcc pillars had also shown a decrease of the yield stress of 10–25% when compared to their bulk nanocrystalline counterparts [33].

3.5. *Comparison of compressed specimens: experiments and molecular dynamics*

When the grain size is significantly smaller than the pillar diameter, deformation will tend to be more homogeneous because the compatibility conditions imparted by the surrounding grains force a more homogeneous deformation mode. The isostrain situation will prevail whereby each grain undergoes the same strain. This is shown in Fig. 8a for a grain size of 20 nm (pillar of 50 nm). The experimental result is for a grain size of 100 nm and pillar diameter of 2 μm. Both MD and experimental results are consistent,

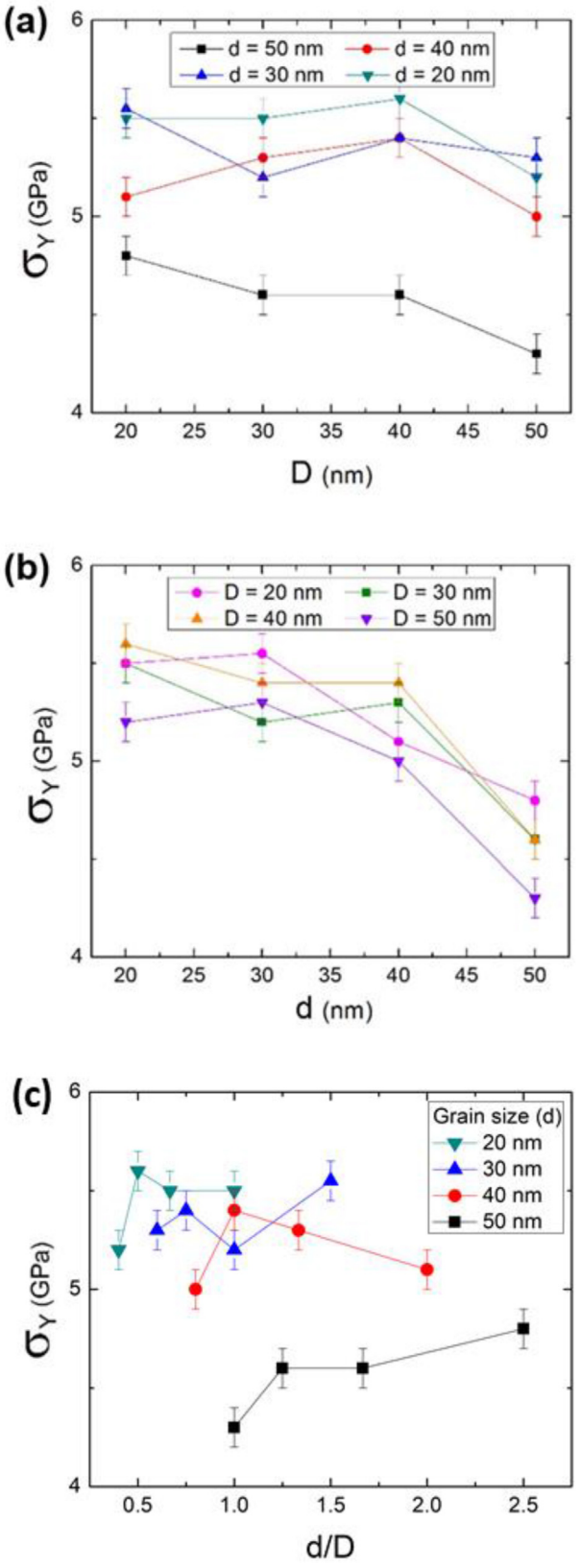

Fig. 7 – Molecular dynamics predictions of yield stress of nanocrystalline tantalum as a function (a) of pillar diameter, D, for different grain sizes, (b) as a function grain size, d, for different pillar diameters, and (c) as a function of the d/D ratio.

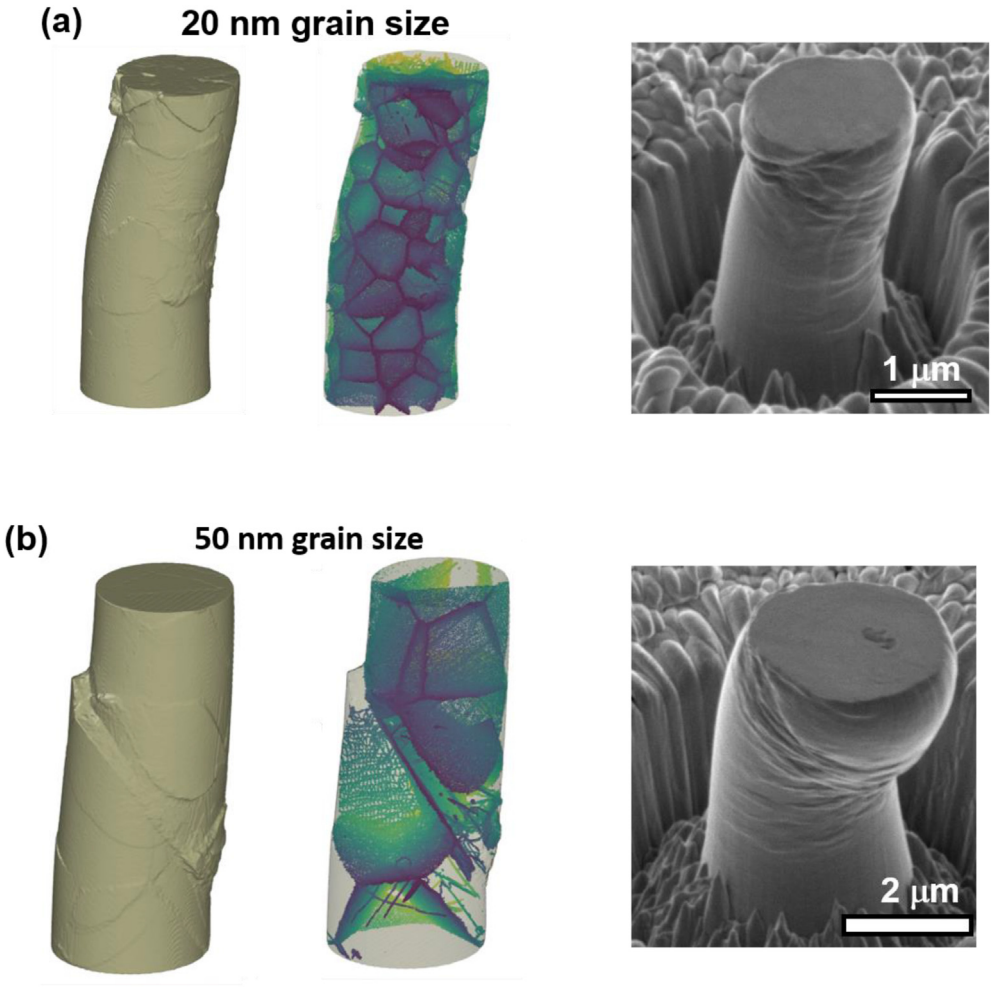

Fig. 8 – Pillar deformation for nanocrystalline specimens; comparison of MD simulations and experiments; although the spatial scales differ by a factor of 100, the same phenomena are observed: (a) when the grain size is much smaller than pillar diameter, homogeneous deformation prevails. (b) When grain size is on the order of pillar diameter, localization of deformation is prevalent.

and the deformation of the pillar walls retains some homogeneity.

The situation is different when the grain size is on the same order as the pillar diameter, Fig. 8b. Localized deformation in a grain is no longer constrained by the surrounding grains. This happens in the experiments, when the grain size is 800 nm (and pillar size of 1 μm) and for the MD simulation when the grain size is 50 nm (and pillar size of 50 nm). Abad et al. [27] also observed localized deformation in Ta monocrystals.

3.6. *Deformation mechanisms predicted by MD*

Detailed examination of the MD deformed microstructures reveals that the pillars undergo plastic deformation through a combination of dislocation activity, grain boundary sliding, and to a lesser extent, twinning. Fig. 9 depicts such scenario, where the example corresponds to a 40 nm diameter pillar with an average grain size of 50 nm. Fig. 9a shows the pillar at the initial stages of plastic deformation (strain ~5%); a few grain-boundary triple junctions are noticeable. Fig. 9b shows a higher magnification highlighting a dislocation loop nucleated at/close to one of these junctions (between GB1, GB2, and GB3). The loop evolves in a [111] direction consistent with glissile dislocations in the bcc structure. Other defects nucleate in the same region as deformation proceeds, as seen in Fig. 9c for a strain of ~5.8%; additional dislocation loops nucleate at grain boundaries and, interestingly, a twin embryo is identified. As deformation continues, the dislocations propagate along [111] until they impinge on another grain boundary or reach a free surface. Fig. 9d shows that for a strain of 6%, the twin embryo has now evolved into a larger twin, while GB3 has become distorted and less recognizable due to plasticity. This twin was also found by automated defect identification through the Crystal Analysis Tool [37], and its output is presented on Fig. 9e. Hagen et al. [36] and Dutta [38] observed twinning when studying iron nanopillars by means of MD simulations. Wang et al. [39] investigated uniaxial compression-induced deformation in 15 nm diameter Ta nanopillars (aspect ratio 6.3) with one grain boundary in various orientations with respect to the loading direction using the Ravelo et al. [40] EAM potential for Ta. Their results suggest that grain-boundary orientation has a

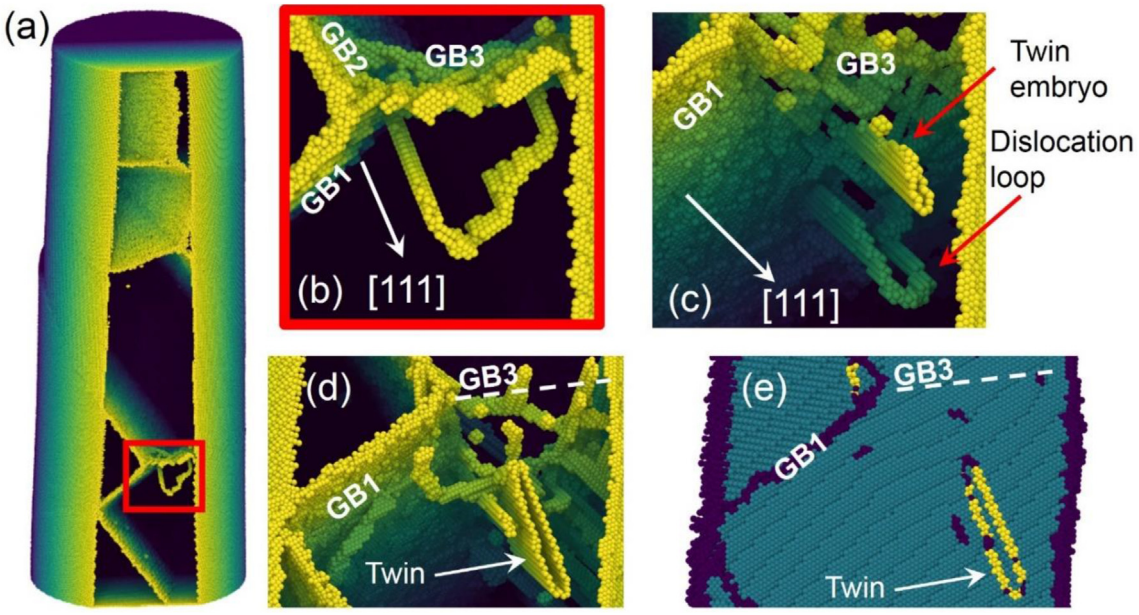

Fig. 9 – MD results: 40 nm diameter pillar with an average grain size of 50 nm. (a) A cut-out of the pillar shows the non-bcc structures for a strain ~0.05, a few triple junctions of grain boundaries are noticeable. (b) magnification of a dislocation loop nucleated close to the GB junction. (c) Detail corresponds to the previous region, now for a strain of ~0.058, more dislocation loops nucleate at grain boundaries and also a twin embryo was identified. (d) At a strain of 0.06, the twin embryo has now evolved into a larger twin. (e) This twin is also found by automated defect identification through the Crystal Analysis Tool [37].

strong effect on the deformation mechanism, the yield stress, the failure strain, and the dislocation dynamics, due to the combined effects of Schmid factors in adjoining crystals and resolved shear stress on the grain boundary plane. Their simulations show twinning, dislocation plasticity, and grain-boundary sliding, highlighting the role of local stress level in the vicinity of the grain boundary and the orientation of the grain boundary in the change of the deformation mechanism taking place. Our yield stresses are slightly below theirs, probably due to our lower strain rate and the availability of a massive amount of nucleation sites. They also report twinning. It is likely that in our case, as in

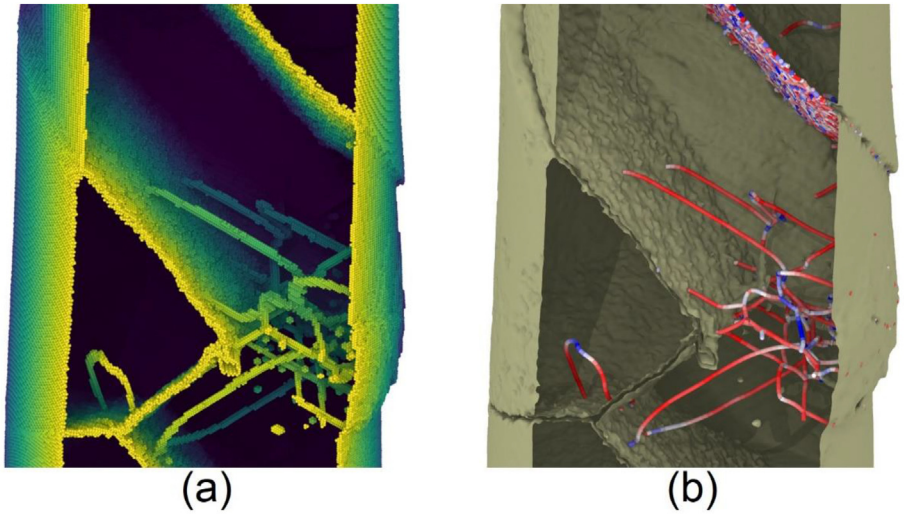

Fig. 10 – MD results: 50 nm grain size, 40 nm diameter pillars, at 0.08 strain. (a) Atoms on non-bcc position filtered by means of the common neighbor analysis [48] indicate the presence of dislocations, grain boundaries and vacancies. (b) Dislocation extraction algorithm output of the atomic positions reveal a dearth of dislocations and low angle grain boundaries (seen as arrangement of dislocations). Color coding of dislocations is according to their type, blue being edge components, and red being screw components, with intermediate color in between. Grain boundary sliding is also visible on the top right hand-side of the pillar.

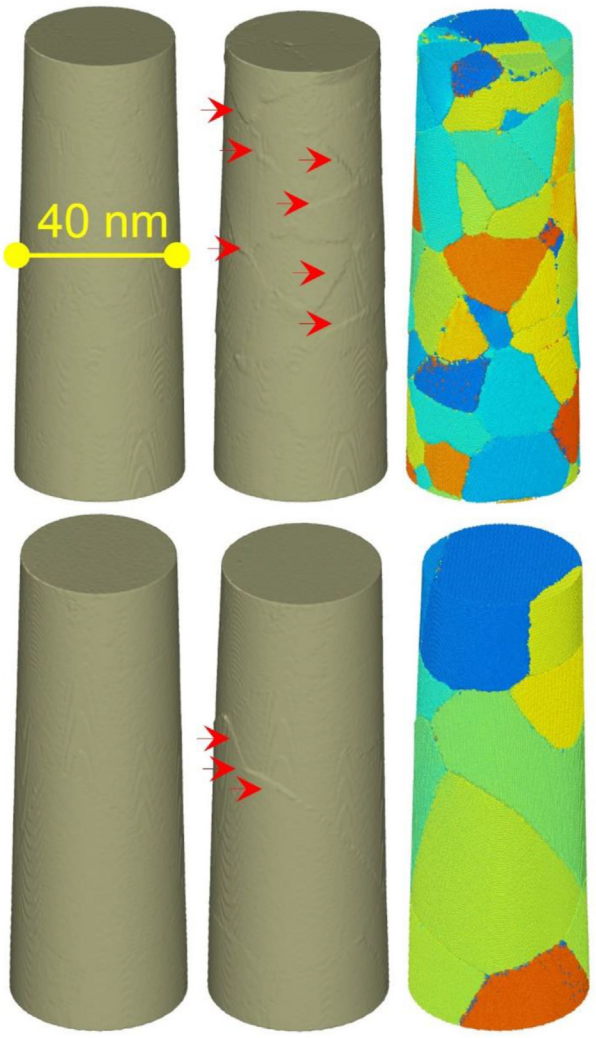

Fig. 11 – MD results: Grain offset evidence for 40 nm diameter pillars of 20 nm grain size (top row) and 50 nm grain size (bottom row). The left column shows the pillar surface at 0 strain. The central column shows the pillar surface at 0.04 strain, with arrows indicating some steps at the surface that turn out to be located at the grain boundaries when comparing with the grain distribution inside the pillar, right column.

theirs, twinning is due to the high strain rates involved. Wang et al. [41], reported twinning in their experiments and simulations of nanoscale crystals of bcc tungsten under compressive loads. The formation of twins in molecular dynamics simulations is promoted by the high strain rate (~10^7/s). The direct comparison with experiments should take this difference into account, since no twinning is observed in the micropillars after deformation.

Weinberger and Cai [42] performed MD and DD simulations on single crystalline fcc and bcc nanopillars (MD) and micropillars (DD) with one pre-existing dislocation. Our yield stresses are within the values reported by them.

The role of triple junctions as plasticity nucleation sites has been previously highlighted by Greer and co-workers in their study of size-dependent deformation of nanocrystalline Pt fcc nanopillars [33]. Fig. 10 shows the microstructure of the same pillar as in Fig. 9, now at a strain of ~8%; it can be seen that several dislocations nucleated at the triple junction inspected, producing a complete distortion of the grain boundary to the point that it can no longer be clearly identified; one can also see that a new dislocation loop nucleated in the vicinity of another triple junction, on the left bottom side of Fig. 10a. The same microstructure was analyzed by means of the dislocation extraction algorithm [22,43] and its output is presented in Fig. 10b. Dislocations are shown as lines with color varying according to their type, from blue corresponding to edge character to red corresponding to a screw portion. As deformation proceeds, the edge portion of the dislocation advances, leaving behind screw dislocations. Quantification by means of the dislocation extraction algorithm reveals that all the pillars have an initial dislocation density in the range of 2 to 5×10^{16} m^{-2} due to a significant amount of grain boundaries represented by an arrangement of dislocations, and that at the maximum strain, the dislocation density is in the range of 3 to 8×10^{16} m^{-2}.

The top right part of Fig. 10b shows that the grain boundary was interpreted as an arrangement of short dislocations and that sliding indeed occurred at this boundary, leaving a step in the outer surface. Grain-boundary sliding was found to be of the Rachinger type [44].

By using a construct surface mesh algorithm built in OVITO, one can analyze the evolution of the surface of the pillars during deformation, and just before dislocation plasticity become noticeable, steps appear on the surface of the pillars, precisely where grain boundaries intersect the pillar contour (Fig. 11). Grain offsets at the surface of pillars were previously reported by Greer and coworkers on Pt [33], and in their experiments on 60 nm grain size Ni pillars [45]. It was also reported by Sun and co-workers in their experiments [46,47] on nanocrystalline Cu micropillars. Grain offsets are a consequence of subtle events of grain boundary sliding and it is likely that this effect contributes to stress concentration at or near triple junctions, favoring nucleation of dislocation in those regions. Since the grain size of the experimental specimens is larger by a factor of 100, one does not expect this sliding to play a significant role.

In situ observation of the deformation mechanism during loading of nanopillars remains an experimental challenge. Hence, atomistic simulations represent an important tool for elucidating deformation mechanisms, provided that simulation results show some degree of consistency with the experimental data. The simulations show that, while in all cases the nanopillars initially underwent non-linear elastic compression, followed by plastic deformation, the subsequent plastic behavior differs depending on the d/D ratio. For d/D well below 1, plastic buckling takes place in a homogeneous deformation pattern, while for d/D around 1 and above, localization of deformation prevails; the deformation of the experiments and the simulations shows the same pattern.

4. Conclusions

This research demonstrates, through a combination of experiments and MD calculations, that the dominating structural

parameter in the plastic response of polycrystalline micropillars is the ratio between the grain size, d, and pillar diameter, D.

- "Small" grain range: If d/D is significantly lower than 1, the deformation in each grain is governed by the generation and annihilation of dislocations at the grain boundaries and the surrounding grains provide efficient compatibility constraints. Thus, the yield strength is to a large extent independent of pillar diameter. The flow stress is governed by the Hall–Petch equation.
- "Large" grain range: If d/D is close to or equal to 1, the deformation is similar to monocrystalline pillars. Dislocation starvation takes place if the mean free path of dislocations is of the same order as the diameter. This yields a dislocation-free crystal, which can have a mechanical response approaching the theoretical shear strength, as has been seen fifty years ago in whiskers [9,10]. As the diameter is increased, a gradual increase in dislocation interaction takes place, leading to a flow stress gradually approaching that of conventional monocrystals. For tantalum, this value is ~50 MPa.
- Molecular Dynamics enabled the identification of three deformation mechanisms, grain-boundary sliding, dislocation mediated plasticity and twinning, with predominance of the first two. Twinning may be an artifact of the much higher strain rates compared to experiments.
- A remarkable qualitative agreement in the deformation characteristics (but not in the stress–strain behavior) between experiments and simulations is observed. Quantitatively, there are significant differences. First, the simulations were performed at a much higher strain rate than used in the experiments. This resulted in a higher flow stress in the simulations as well in differences in the stress strain response. Second, there is a factor of 100 spatial scale difference between the experiments (μm) and MD (nm). Third, although the pillars were extracted from nanocrystals with an average grain size, there are local variations. Hence, a pillar with a given d/D ratio may contain regions with larger or smaller d/D. Depending on the statistical distribution of grain sizes, this distribution can generate a range in grain-boundary strengths. The comparison of experimental observations and molecular dynamics simulations is therefore limited by the large spatial and temporal differences.

Declaration of Competing Interest

The author declares no conflict of interest.

Acknowledgement

This research is funded by a UC Research Laboratories Grant (09-LR-06-118456-MEYM) and was performed under the auspices of the U.S. Department of Energy by Lawrence Livermore National Laboratory under Contract DE-AC52-07NA27344. The visit of MAM to Germany was supported by the Humboldt Foundation Award to one of us (MM). Carlos J Ruestes was supported by SiiP-UNCUYO and ANPCyT PICT 2018-0773. Simulations were conducted at TOKO-FCEN-UNCUYO and Mendieta-CCAD-UNC computing cluster. We thank Professor Peter Hosemann, UC Berkeley, for allowing us to use his nanoindentation machine.

REFERENCES

[1] Uchic MD, Dimiduk DM, Florando JN, Nix WD. Sample dimensions influence strength and crystal plasticity. Science 2004;305:986–9.
[2] Greer JR, Oliver WC, Nix WD. Size dependence of mechanical properties of gold at the micron scale in the absence of strain gradients. Acta Mater 2005;53:1821–30.
[3] Ashby MF. The deformation of plastically non-homogeneous materials. Philos Mag 1970;21:399–424.
[4] Aifantis EC. On the role of gradients in the localization of deformation and fracture. Int J Eng Sci 1992;30:1279–99.
[5] Nix WD, Gao H. Indentation size effects in crystalline materials: a law for strain gradient plasticity. J Mech Phys Solid 1998;46:411–25.
[6] Fleck NA, Muller GM, Ashby MF, Hutchinson JW. Strain gradient plasticity: theory and experiment. Acta Metall Mater 1994;42:475–87.
[7] Kim JY, Jang D, Greer JR. Tensile and compressive behavior of tungsten, molybdenum, tantalum and niobium at the nanoscale. Acta Mater 2010;58:2355–63.
[8] Budiman AS, Han SM, Greer JR, Tamura N, Patel JR, Nix WD. A search for evidence of strain gradient hardening in Au submicron pillars under uniaxial compression using synchrotron X-ray microdiffraction. Acta Mater 2008;56:602–8.
[9] Brenner SS. Tensile strength of whiskers. J Appl Phys 1956;27:1484–91.
[10] Brenner SS. Plastic deformation of copper and silver whiskers. J Appl Phys 1957;28:1023–6.
[11] Lu CH, Remington BA, Maddox BR, Kad B, Park HS, Prisbrey ST, et al. Laser compression of monocrystalline tantalum. Acta Mater 2012;60:6601–20.
[12] Lu CH, Remington BA, Maddox BR, Kad B, Park HS, Kawasaki M, et al. Laser compression of nanocrystalline tantalum. Acta Mater 2013;61:7767–80.
[13] Zhilyaev AP, Langdon TG. Using high-pressure torsion for metal processing: fundamentals and applications. Prog Mater Sci 2008;53:893–979.
[14] Zepeda-Ruiz LA, Stukowski A, Oppelstrup T, Bulatov VV. Probing the limits of metal plasticity with molecular dynamics simulations. Nature 2017;550:492.
[15] Hirel P. Atomsk: a tool for manipulating and converting atomic data files, Comput. Phys. Commun. 2015;197:212–9.
[16] Kelchner CL, Plimpton S. Dislocation nucleation and defect structure during surface indentation. Phys Rev B Condens Matter 1998;58:11085.
[17] Dai XD, Kong Y, Li JH, Liu BX. Extended Finnis-Sinclair potential for bcc and fcc metals and alloys. J Phys Condens Matter 2006;18:4527.
[18] Remington TP, Ruestes CJ, Bringa EM, Remington BA, Lu CH, Kad B, et al. Plastic deformation in nanoindentation of tantalum: a new mechanism for prismatic loop formation. Acta Mater 2014;78:378–93.
[19] Ruestes CJ, Stukowski A, Tang Y, Tramontina DR, Erhart P, Remington BA, et al. Atomistic simulation of tantalum nanoindentation: effects of indenter diameter,

penetration velocity, and interatomic potentials on defect mechanisms and evolution. Mater Sci Eng A 2014;613:390–403.
[20] Tang Y, Bringa EM, Meyers MA. Inverse Hall-Petch relationship in nanocrystalline tantalum. Mater Sci Eng A 2013;580:414–26.
[21] Plimpton S. Fast parallel algorithms for short-range molecular dynamics. J Comput Phys 1995;117:1–19.
[22] Stukowski A, Albe K. Extracting dislocations and non-dislocation crystal defects from atomistic simulation data. Model Simulat Mater Sci Eng 2010;18:085001.
[23] Figueiredo RB, Sabbaghianrad S, Giwa A, Greer JR, Langdon TG. Evidence for exceptional low temperature ductility in polycrystalline magnesium processed by severe plastic deformation. Acta Mater 2017;122:322–31.
[24] Maury N, Zhang NX, Huang Y, Zhilyaev AP, Langdon TG. A critical examination of pure tantalum processed by high-pressure torsion. Mater Sci Eng A 2015;638:174–82.
[25] Wei Q, Pan ZL, Wu XL, Schuster BE, Kecskes LJ, Valiev RZ. Microstructure and mechanical properties at different length scales and strain rates of nanocrystalline tantalum produced by high-pressure torsion. Acta Mater 2011;59:2423–36.
[26] Ligda J, Scotto D'Antuono D, Taheri ML, Schuster BE, Wei Q. Quasi-static tensile and compressive behavior of nanocrystalline tantalum based on miniature specimen testing—Part I: materials processing and microstructure. JOM 2016;68:2832–8.
[27] Torrents Abad O, Wheeler JM, Michler J, Schneider AS, Arzt E. Temperature-dependent size effects on the strength of Ta and W micropillars. Acta Mater 2016;103:483–94.
[28] Mitchell TE, Spitzig WA. Three-stage hardening in tantalum single crystals. Acta Metall 1965;13:1169–79.
[29] Zerilli FJ, Armstrong RW. Dislocation-mechanics-based constitutive relations for material dynamics calculations. J Appl Phys 1987;61:1816–25.
[30] Zerilli FJ, Armstrong RW. Description of tantalum deformation behavior by dislocation mechanics based constitutive relations. J Appl Phys 1990;68:1580–91.
[31] Mordike BL, Rudolph G. Three-stage hardening in tantalum deformed in compression. J Mater Sci 1967;2:332–8.
[32] Girault B, Schneider AS, Prick CP, Arzt E. Strength effects in micropillars of a dispersion strengthened superalloy. Adv Eng Mater 2010;12:385–8.
[33] Gu XW, Loynachan CN, Wu Z, Zhang YW, Srolovitz DJ, Greer JR. Size-dependent deformation of nanocrystalline Pt nanopillars. Nano Lett 2012;12:6385–92.
[34] Chen XX, Ngan AHW. Specimen size and grain size effects on tensile strength of Ag microwires. Scripta Mat 2011;64:717–20.
[35] Yuan L, Xu C, Shivpuri R, Shan D, Guo B. Size effect in the uniaxial compression of polycrystalline Ni nanopillars with small number of grains. Metall Mater Trans 2019;50:4462–79.
[36] Hagen AB, Snartland BD, Thaulow C. Temperature and orientation effects on the deformation mechanisms of α-Fe micropillars. Acta Mater 2017;129:398–407.
[37] Stukowski A, Bulatov VV, Arsenlis A. Automated identification and indexing of dislocations in crystal interfaces. Model Simulat Mater Sci Eng 2012;20:085007.
[38] Dutta A. Compressive deformation of Fe nanopillar at high strain rate: modalities of dislocation dynamics. Acta Mater 2017;125:219–30.
[39] Wang L, Zhao F, Zhao FP, Cai Y, An Q, Luo SN. Grain boundary orientation effects on deformation of Ta bicrystal nanopillars under high strain-rate compression. J Appl Phys 2014;115:053528.
[40] Ravelo R, Germann TC, Guerrero O, An Q, Holian BL. Shock-induced plasticity in tantalum single crystals: interatomic potentials and large-scale molecular-dynamics simulations. Phys Rev B Condens Matter 2013;88:134101.
[41] Wang J, Zeng Z, Weinberger CR, Zhang Z, Zhu T, Mao SX. In situ atomic-scale observation of twinning-dominated deformation in nanoscale body-centred cubic tungsten. Nat Mater 2015;14:594.
[42] Weinberger CR, Cai W. Surface-controlled dislocation multiplication in metal micropillars. Proc. Natl. Acad. Sci. 2008;105:14304–7.
[43] Stukowski A. Visualization and analysis of atomistic simulation data with OVITO-the Open Visualization Tool. Model Simulat Mater Sci Eng 2010;18:015012.
[44] Langdon TG. Grain boundary sliding revisited: developments in sliding over four decades. J Mater Sci 2006;41:597–609.
[45] Jang D, Greer JR. Size-induced weakening and grain boundary-assisted deformation in 60 nm grained Ni nanopillars. Scr. Mater. 2011;64:77–80.
[46] Zhang JY, Liang X, Zhang P, Wu K, Liu G, Sun J. Emergence of external size effects in the bulk-scale polycrystal to small-scale single-crystal transition: a maximum in the strength and strain-rate sensitivity of multicrystalline Cu micropillars. Acta Mater 2014;66:302–16.
[47] Zhang JY, Liu G, Sun J. Comparisons between homogeneous boundaries and heterophase interfaces in plastic deformation: nanostructured Cu micropillars vs. nanolayered Cu-based micropillars. Acta Mater 2013;61:6868–81.
[48] Faken D, Jónsson H. Systematic analysis of local atomic structure combined with 3D computer graphics. Comput Mater Sci 1994;2:279–86.